

# Generalized Contact Constraints of Hybrid Trajectory Optimization for Different Terrains and Analysis of Sensitivity to Randomized Initial Guesses

Kenneth Chao<sup>1</sup> and Pilwon Hur<sup>1</sup>

**Abstract**—To generate a dynamic bipedal walking with foot rolling motion for bipedal robot, hybrid trajectory optimization is capable of planning level walking with great energetic efficiency. However, the direct implementation of this optimization requires different sets of variables to express different active contact constraints, which can be complicated to implement. To simplify the optimization formulation, we propose the generalized contact constraints where the same set of variables are used through all the walking phases. By changing the variable and constraint bounds, different contact constraints for different contact conditions can be generally expressed. The proposed modifications are applied on the bipedal robot AMBER 3, where the optimization results on different terrains are compared and discussed. On the other hand, it is known that a randomized initial guess can be used to solve this optimization, yet its effect on the gaits on different terrains is unclear. As a result, we analyzed the sensitivity of the optimization to a set of randomized initial guesses. The level and downslope walking gaits are also validated via the experiments on AMBER 3.

## I. INTRODUCTION

Generating a dynamic bipedal walking gait which lets bipedal robots walk like humans has been a milestone that is yet to be achieved. Among various characteristics in human walking, the great energetic efficiency in terms of low Cost of Transport (COT) [3] and foot rolling motion are two remarkable ones. Though it has been achieved by underactuated bipedal robots [9], it is even more challenging to implement those features on the bipedal robots that have the control authority to actively switch between different actuation types. To enable the bipedal robot AMBER 3 (Fig. 1) to perform such complex dynamic behavior, trajectory optimization with direct collocation is a powerful framework to generate the dynamic walking for high dimensional bipedal systems.

For solving the walking gait with multiple phases in particular, there are two main state-of-the-art approaches: trajectory optimization through contact [10], [4], [8] and hybrid trajectory optimization [5], [6], [14]. With no need to specify the contact sequence, trajectory optimization through contact (or contact-implicit trajectory optimization), proposed by Posa et al. [10], simultaneously optimizes all the states, controls and contact forces of all the potential contact points, where the problem is formulated as a nonlinear optimization with complementary constraints. However, the relaxation of complementary constraints with nonlinear solvers such as SNOPT or IPOPT needs to be handled carefully for a target

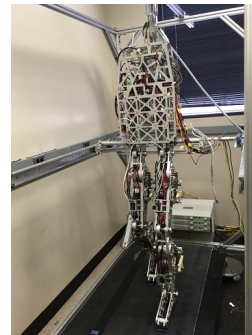


Fig. 1: The human-sized planar bipedal robot AMBER 3 (left). It is 148 cm tall, weights 33.4 kg, with active hip, knee and ankle joints and passive toes and heels.

environment [10], [4], [8], which makes this method more complicated to be adopted when the gait parameter or terrain profile is changed.

On the other hand, hybrid trajectory optimization (e.g., the gait optimization method proposed by Hereid et al. [5], [6] to optimize the hybrid zero dynamics (HZD) [13], [12]) requires a predefined contact sequence. One important merit of this approach is that it is less sensitive to the initial guess (as the optimization can be solved with a randomized initial guess [6]). To efficiently achieve dynamic walking generation on various terrains and gait parameters, we adopt the hybrid trajectory optimization, which is introduced in Section III. In Section IV we present the generalized contact constraints which can be used for all contact conditions and different terrains (including slopes and stairs). In Section V, the optimization results for different terrains are compared and discussed. The sensitivity of this framework to randomized initial guesses, and the experimental results of level walking and downslope walking as validations are shown. Conclusions and future work are presented in Section VI.

## II. BIPEDAL LOCOMOTION AS A HYBRID SYSTEM

For a bipedal locomotion system, it can be described as a *hybrid system*, which contains both continuous and discrete dynamics. A **domain** (or a walking phase) in general is specified with a set of contact conditions across possible contact points. The continuous dynamics is used to describe the system behavior in a domain. The discrete dynamics is used to describe the state transition from one domain to another, where the **guard** defines the state condition to trigger the state transition.

<sup>1</sup>Kenneth Y. Chao and Pilwon Hur are with the Department of Mechanical Engineering, Texas A&M University, 3123 TAMU, College Station, TX 77843, USA. {kchao, pilwonhur}@tamu.edu

**Continuous Dynamics.** The dynamics of a rigid body model can be expressed as follows:

$$D(q)\ddot{q} + C(q, \dot{q})\dot{q} + G(q) = Bu + J^T\lambda \quad (1)$$

where  $q$  is the generalized coordinate,  $D(q)$  is the inertia matrix,  $C(q, \dot{q})$  is the Coriolis matrix,  $G(q)$  is the gravity vector,  $J$  is the Jacobian matrix of the contact position  $\phi(q)$  such that  $J = \partial\phi/\partial q$ ,  $B$  is the torque distribution matrix,  $u$  is the control input, and  $\lambda$  is the contact force. The contact position in 2D can be described as  $\phi(q) = [\phi_x(q), \phi_z(q)]^T$ , where  $x$  is the horizontal axis and  $z$  is the vertical axis.

**Discrete Dynamics.** When the contact condition of the system is changed (e.g., a new contact is achieved or a existing contact breaks), the state of the system will have a discrete change. A classic example is the joint velocity change due to the impact induced by heel-strike (or foot-strike). Following the hypothesis listed in [12], the equations governing the kinematics and dynamics about a *new established contact* can be expressed as:

$$\begin{bmatrix} D(q^-) & -J_e^T \\ J_e & 0 \end{bmatrix} \begin{bmatrix} \dot{q}^+ \\ \delta F_{impact} \end{bmatrix} = \begin{bmatrix} D(q^-)\dot{q}^- \\ 0 \end{bmatrix} \quad (2)$$

where the superscript '+' denotes the post-impact state, the superscript '-' denotes the pre-impact state,  $D(\cdot)$  is the inertia matrix (note  $D(q^-) = D(q^+)$ ),  $J_e$  is the Jacobian matrix of the new established contact point, and  $\delta F_{impact}$  is the impact impulse. The first row of Eq. (2) is the momentum equation during impact, and the second row is the velocity of the new established contact position. For the case where only the existing contact breaks, the state continuity holds (i.e.,  $q^- = q^+$  and  $\dot{q}^- = \dot{q}^+$ ) as no impact is induced.

### III. HYBRID TRAJECTORY OPTIMIZATION FOR WALKING WITH MULTIPLE CONTACT PHASES ON FLAT GROUND

In this section, the method of trajectory optimization using direct collocation for hybrid systems with multiple domains will be introduced. To establish the hybrid trajectory optimization, the contact sequence needs to be specified, and the trajectory is divided to several domains.

#### A. Contact Sequence from Human Data

When a stable periodic gait with multiple domains reaches the steady state, the order of phases and the transitions in general will be fixed and periodic; therefore, it enables the usage of a predetermined contact sequence to solve the hybrid trajectory optimization. We are using the contact sequence shown in Fig. 2, which is similar to the sequence used in [6]:

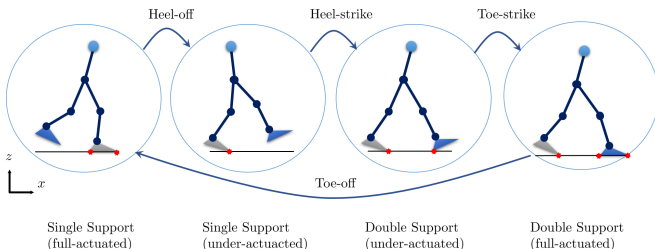


Fig. 2: The schematic (a directed graph) of the contact sequence from human data.

#### B. Hermite-Simpson Collocation

In our direct collocation, the Hermite-Simpson method is used, where all the joint variables  $q$ ,  $\dot{q}$ ,  $\ddot{q}$  are discretized as nodes of cubic-splines. The Hermite-Simpson constraint  $H_{HSM}(\cdot)$  for relating the states in adjacent collocation points  $k-1$  to  $k+1$  (where  $k$  is an even number) in the domain  $n$  can be stated as:

$$\begin{aligned} x_k - \frac{1}{2}(x_{k+1} + x_{k-1}) - \frac{1}{8}\Delta t_n(\dot{x}_{k-1} - \dot{x}_{k+1}) &= 0 \\ x_{k+1} - x_{k-1} - \frac{1}{6}\Delta t_n(\dot{x}_{k-1} + 4\dot{x}_k + \dot{x}_{k+1}) &= 0 \end{aligned} \quad (3)$$

where  $x_k = [q_k, \dot{q}_k]^T$ , and  $\Delta t_n$  is the time step in the domain  $n$ . Please refer to [2], [7], [6] for more information.

#### C. Constrained Dynamics

At each collocation point, given the joint state variables  $q$ ,  $\dot{q}$ ,  $\ddot{q}$ , the control  $u$ , and ground reaction forces  $\lambda$  at the active contact point(s)  $\phi(q)$ , the constraints of constrained dynamics  $H_{CDym}(\cdot)$  can be expressed as follows:

$$\begin{cases} D(q)\ddot{q} + C(q, \dot{q})\dot{q} + G(q) - Bu - J^T\lambda = 0 \\ J\ddot{q} + \dot{J}\dot{q} = 0 \end{cases} \quad (4)$$

#### D. Setup of Other Constraints

In this section, the other important building blocks of the hybrid trajectory optimization for multi-domain bipedal walking will be introduced. Starting from the contact constraints for contact dynamics (for the 2D case, which can be readily extended to 3D [10]), the boundary constraints and periodic constraints relating boundary collocation points between domains will be explained.

**Contact Constraints for Flat Ground.** For each active contact point  $\phi(q)$  with corresponding contact force  $\lambda_x$  and  $\lambda_z$ , assuming the contact position is non-sliding, a set of equalities and inequalities  $H_{Contact}(\cdot)$  can be used to describe the Coulomb friction model (for the 2D case):

$$\begin{cases} \lambda_z \geq 0, & \infty \geq \lambda_x \geq -\infty \\ \mu\lambda_z - |\lambda_x| \geq 0 \\ \phi_z(q) = 0 \\ J\dot{q} = 0 \end{cases} \quad (5)$$

where  $\mu$  is the friction coefficient,  $\phi_z(q)$  is the normal distance from the contact point to the contact surface, and  $J$  is the Jacobian matrix of the contact point position  $\phi(q)$ .

**Guard Constraints.** When a contact is about to be achieved, the guard constraints  $H_{Guard}(\cdot)$  can be expressed as:

$$\begin{cases} \phi_z(q) = 0 \\ J_z\dot{q} \leq 0 \end{cases} \quad (6)$$

**Boundary Constraints.** As we introduced in the previous section about the discrete dynamics (Eq. (2)), the boundary constraints of collocation points between each domain  $H_{Boundary}(\cdot)$  can be expressed as:

$$\begin{aligned} \infty \geq \delta F_{impact_x} \geq -\infty, & \quad \delta F_{impact_z} \geq 0 \\ \begin{cases} q^+ - q^- = 0 \\ D(q^-)(\dot{q}^+ - \dot{q}^-) - J_e^T\delta F_{impact} = 0 \end{cases} & \end{aligned} \quad (7)$$

<sup>1</sup>Starting from this section, for simplicity the subscript  $k$  for every free variables at node (collocation point)  $k$  is omitted, e.g.,  $x_k \rightarrow x$ ,  $q_k \rightarrow q$ .

where  $\delta F_{impact} = [\delta F_{impact_x}, \delta F_{impact_z}]^T$  in 2D. Note the constraint  $J_e \dot{q}^+ = 0$  is already imposed as part of the contact constraint in the next domain in Eq. (5).

**Periodic Constraints.** The periodic condition  $H_{Periodic}(\cdot)$  is the slightly modified boundary constraint shown below:

$$\begin{aligned} \infty &\geq \delta F_{impact_x} \geq -\infty, \quad \delta F_{impact_z} \geq 0 \\ \begin{cases} R(q_{start}) - q_{end} = 0 \\ D(q_{end})(R(\dot{q}_{start}) - \dot{q}_{end}) - J_e^T \delta F_{impact} = 0 \\ x_{com}(q_{end}) - x_{com}(q_{start}) \geq d_{min} \end{cases} \end{aligned} \quad (8)$$

where  $R$  is the relabeling matrix to swap joint variables between legs and  $d_{min}$  is the minimum horizontal traveling distance of the center of mass position  $x_{com}$ .

**Cost Function for Multi-phases.** Similar to other works [6], [10], the Cost of Transport (COT) is chosen as the objective function. Using Simpson's quadrature rule to calculate the integral, the cost in a domain  $n$  can be expressed as:

$$J_n(X) = \sum_{j=1}^{M_n} \omega_j P(u_j, \dot{q}_j), \quad (9)$$

$$\omega_i = \begin{cases} \frac{1}{6} \Delta t_n & \text{if } j = 1 \text{ or } j = M_n \\ \frac{2}{3} \Delta t_n & \text{if } j \text{ is even} \\ \frac{1}{3} \Delta t_n & \text{else} \end{cases} \quad (10)$$

where  $\Delta t_n$  is the time step in the domain  $n$  (i.e., the time duration between collocation point  $k-1$  and  $k+1$  in Eq. (3)),  $M_n$  (an odd number) is the number of collocation points in the domain  $n$  ( $n \in [1, 2, \dots, N]$ ), and  $P(\cdot)$  is the summation of the absolute values of the power consumption of all actuators. The overall cost then can be calculated as:

$$J(X) = \frac{1}{mgd} \sum_{n=1}^N J_n(X) \quad (11)$$

where  $mg$  is the robot weight,  $d$  is the traveling distance.

### E. Optimization Formulation

Assuming the target system has  $N$  domains and  $M$  collocation points, the set of free variables  $X$  is defined as  $\{q_i, \dot{q}_i, \ddot{q}_i, u_i, \lambda_i, \gamma_i, \delta F_{impact_n}, \Delta t_n\}$  for all  $i \in [1, 2, \dots, M]$ ,  $n \in [1, 2, \dots, N]$ , and the hybrid trajectory optimization can be expressed as the following:

$$\begin{aligned} X^* &= \underset{X}{\operatorname{argmin}} J(X) \\ \text{s.t.} \quad & X_{lb} \leq X \leq X_{ub} \\ & H_{eq}(X) = 0 \\ & H_{iq}(X) \geq 0 \end{aligned} \quad (12)$$

where  $X_{lb}$  and  $X_{ub}$  are the lower bound and upper bound of  $X$ .  $H_{eq}(\cdot)$  and  $H_{iq}(\cdot)$  are the collections of equality and inequality constraints introduced in Eqs. (3) to (8).

## IV. GENERALIZED CONTACT CONSTRAINTS OF HYBRID TRAJECTORY OPTIMIZATION FOR MULTIPLE DOMAINS AND DIFFERENT TERRAINS

The hybrid trajectory optimization introduced in the previous section provides a systematic framework that can generate efficient walking gait with multiple phases, which has

been validated by 3D humanoid robot DURUS [6]. However, the direct implementation of the formulation described in Eq. (12) can be complicated because the contact constraints in  $H_{contact}(\cdot)$  are imposed for different contact points or different numbers of contact points in different domains, and only the level walking was tested in the previous works [5], [6]. In this section, we will introduce the contact constraints that can be generally used in any domain (where only the constraint or variable bounds need to be varied) and different terrains (including stairs or ramps).

### A. Contact Constraints Inspired by Optimization through Contact

To simplify the optimization problem and improve its sparsity, we adopt a scheme similar to the one depicted in [10]. By introducing a few slack variables, we replace the absolute value and the normal velocity at the active contact points in Eq. (5) as follows:

$$H_{ActiveContact}(\cdot) = \begin{cases} \lambda_z, \lambda_x^-, \lambda_x^+ \geq 0, \quad \gamma = 0 \\ \mu \lambda_z - \lambda_x^- - \lambda_x^+ \geq 0 \\ \phi_z(q) = 0 \\ \gamma - J\dot{q} = 0 \end{cases} \quad (13)$$

where  $\lambda_x^- + \lambda_x^+ = |\lambda_x|$  and  $-\lambda_x^- + \lambda_x^+ = \lambda_x$ . On the other hand, the constraints for inactive contact points can be expressed as :

$$H_{InactiveContact}(\cdot) = \begin{cases} \lambda_z, \lambda_x^-, \lambda_x^+ = 0, \quad \infty \geq \gamma \geq -\infty \\ \mu \lambda_z - \lambda_x^- - \lambda_x^+ = 0 \\ \phi_z(q) \geq 0 \\ \gamma - J\dot{q} = 0 \end{cases} \quad (14)$$

The constraints for inactive contact points seem redundant by intuition, but its insertion to the optimization has the following benefits:

- 1) This can simplify the formulation of both constrained dynamics and contact constraints because the only difference between the active and inactive contact constraints are their constraint and variable bounds. Therefore, the same dynamic equations and the same contact constraints can be generally expressed in every domain for all the possible contact conditions.
- 2) Similar to the separated form of Hermite-Simpson method [2], this method can slightly improve the sparsity of the optimization by introducing extra free variables.
- 3) On the other hand, without changing the constraint expression, the contact constraint can also be modified to express the constraints at the guard (when a contact is about to be achieved):

$$H_{Guard}(\cdot) = \begin{cases} \lambda_z, \lambda_x^-, \lambda_x^+ = 0, \quad \gamma_z \leq 0, \quad \infty \geq \gamma_x \geq -\infty \\ \mu \lambda_z - \lambda_x^- - \lambda_x^+ = 0 \\ \phi_z(q) = 0 \\ \gamma - J\dot{q} = 0 \end{cases} \quad (15)$$

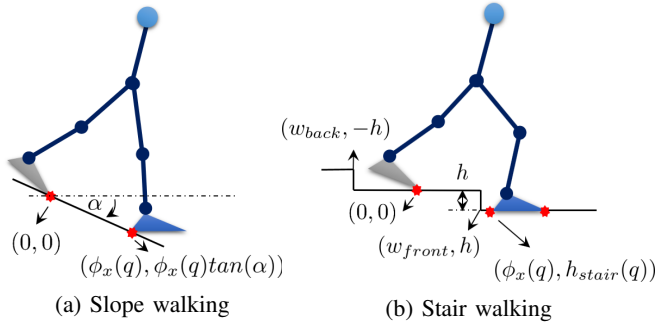


Fig. 3: The schematics of slope walking and stair walking.

### B. Contact Constraints for Ramps and Stairs

With the contact constraints that can generally apply to any domain for flat terrain, the next step is to extend it for other terrains. This can be achieved by redefining the height from the contact point to the contact surface  $\phi_z(q)$  in the contact constraints Eq. (13), Eq. (14) and Eq. (15). As shown in Fig. 3 (a) and (b), assuming the origin is at the toe of the trailing leg, then a ramp profile can be expressed with the slope angle  $\alpha$ , and a stair profile can be described with the stair height  $h$ , and  $w_{front}$  and  $w_{back}$  which are related to the stair width. The general expression of  $\phi_z(q)$  then can be derived as follows:

$$\Phi(q) = \phi_z(q) - \phi_x(q)\tan(\alpha) - h_{stair}(q) \quad (16)$$

$$\begin{cases} \Phi_z(q) = 0 & \forall H_{ActiveContact}(\cdot) \\ \Phi_z(q) \geq 0 & \forall H_{InactiveContact}(\cdot) \\ \Phi_z(q) = 0 & \forall H_{Guard}(\cdot) \end{cases}$$

where

$$h_{stair}(q) = \begin{cases} -h & \text{if } \phi_x(q) < w_{back} \\ 0 & \text{if } w_{front} \geq \phi_x(q) \geq w_{back} \\ h & \text{if } \phi_x(q) > w_{front} \end{cases} \quad (17)$$

With this expression, Fig. 3 (a) becomes the special case with  $h = 0$  and Fig. 3 (b) is the case with  $\alpha = 0$ . In this way, the targeted terrain of the gait optimization can be easily changed by adjusting those parameters based on the terrain profile.

## V. OPTIMIZATION RESULTS

In this section, by using the proposed contact constraints, the optimization results of bipedal walking on flat ground, different slopes and stairs are presented. Starting from the optimization setup, the remarks of the optimization results on different terrains and the related optimization sensitivity to the random initial guesses will be presented and discussed.

TABLE I: Details of the gait optimization with proposed contact constraints for bipedal robot AMBER 3.

Free variable #	2355	Constraint #	2721
Equality constraints #	1927	Inequality constraints #	794
Domain #	4	Node # in domains	[21,21,21,5]
Objective function	COT	Jacobian sparsity	0.4%

### A. Optimization Setup

We use IPOPT with the linear `ma57` solver and its MATLAB interface for the optimization implementation. The expression of constraints and their analytical Jacobian matrices are derived using Wolfram Mathematica, where the matrices are expressed in the form of sparse matrices. The optimization summary is shown in Table I. For all the results, the order of the domains and the corresponding contact conditions are depicted in Fig. 2, and the time step for each domain  $\Delta t_n$  is constrained within  $[1e-5, 0.5]$ . To reduce the torso swaying, the torso angle is constrained within  $[-0.15, 0.15]$  rad (for slope walking the range is  $[-\alpha, \alpha]$  rad where  $\alpha$  is the slope angle).

### B. Gait Optimization on Different Terrains

In this section, we present our main result – walking on different terrains (flat ground, ramps and stairs) generated from the introduced optimization framework for AMBER 3. Note all the optimization results are the periodic gaits.

To generate the optimization results also analyze the optimization sensitivity to randomized initial guesses, we ran the same optimization for each terrain with 200 randomized initial guesses, and then picked the solution with the lowest COT. The cost of transport, walking speed, and time step in each domain ( $\Delta t_n$ ) of the optimization results are listed in Table II. In the following the remarks of generated gaits on different terrains will be presented and discussed.

**Flat-ground walking.** Among walking on different terrains, level walking with multi-domain has the lowest COT 0.096. The extremely small fourth  $\Delta t_n$  in the fourth column of Table II indicates that the toe-strike of the front leg and the toe-off of the trailing leg happen almost at the same time.

**Slope walking.** Compared to level walking, it is shown that for slope walking (Fig. 4), the larger the slope angle ( $|\alpha|$ ), the larger the COT. The optimization results in Table II also indicate that the gait on ramp ascent with the same slope angle generally requires larger COT than the ramp descent. Another finding of the comparison between upslope and downslope walking is that upslope walking tends to have a smaller torso swaying, as the torso swaying on upslope requires more energy to work against the gravity. In addition, it is found that when the slope angle becomes larger, the fourth  $\Delta t_n$  in Table II becomes much greater than  $1e-5$ .

**Stair walking.** Fig. 5 shows the optimization result of stair walking ascent and descent. One obvious difference between stair walking and other gaits is that the third  $\Delta t_n$  for stair walking in Table II is smaller so that the front foot achieves flat contact more quickly. To demonstrate the capability of the optimization framework for generating stair walking, we only tried a few terrain profiles for two reasons. First, compared to the slope walking, stair walking is more complicated to solve, as the contact constraints for stair walking are not smooth. Second, the biomechanics study of stair walking [11] indicates that in stair walking the forefoot strikes the ground first, which is different from the sequence we used. To get better optimization results for stair walking, the contact sequence must be modified accordingly.

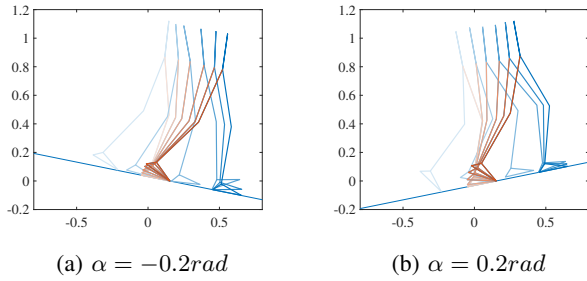


Fig. 4: The walking tiles of slope walking.

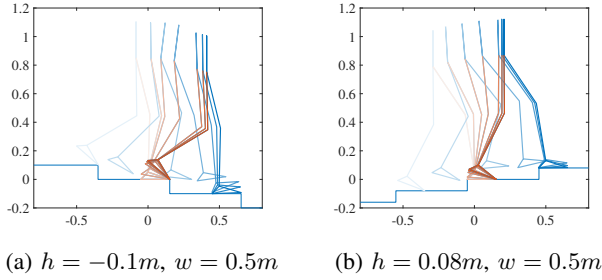


Fig. 5: The walking tiles of stair walking.

TABLE II: The summary of optimization results on different terrains

Terrain	COT	Step time (s)	$\Delta t_n$ (s)
Flat ground	0.096	1.35	[0.030, 0.030, 0.014, $1e-5$ ]
Ramp descent ( $\alpha = -0.1rad$ )	0.121	1.48	[0.030, 0.03, 0.021, $1e-5$ ]
Ramp descent ( $\alpha = -0.2rad$ )	0.214	1.59	[0.030, 0.030, 0.023, 0.023]
Ramp ascent ( $\alpha = 0.1rad$ )	0.170	1.39	[0.030, 0.030, 0.016, $1e-5$ ]
Ramp ascent ( $\alpha = 0.2rad$ )	0.266	1.58	[0.030, 0.030, 0.022, 0.028]
Stair descent ( $h = -0.1m, w = 0.5m$ )	0.356	1.20	[0.030, 0.030, 0.006, $1e-5$ ]
Stair ascent ( $h = 0.08m, w = 0.5m$ )	0.357	1.16	[0.030, 0.030, 0.004, $1e-5$ ]

### C. Optimization Sensitivity to Randomized Initial Guesses

In this subsection, we present and discuss the optimization sensitivity to the initial guess. Because the formulated optimization is nonlinear and non-convex, a solver like IPOPT will return a local optimal solution rather than a global one. As a result, the initial guess for  $X$  in Eq. (12) can have a significant effect on the optimization result. Though in [6] it is mentioned that this optimization framework can be used with a randomized initial guess, it is still not clear how well a randomized initial guess can be used for different terrains, and a good initial condition for the gait with the complex contact sequence can be hard to derive. To get more understanding about the optimization sensitivity to randomized initial guesses, in Fig. 6 we show the histograms

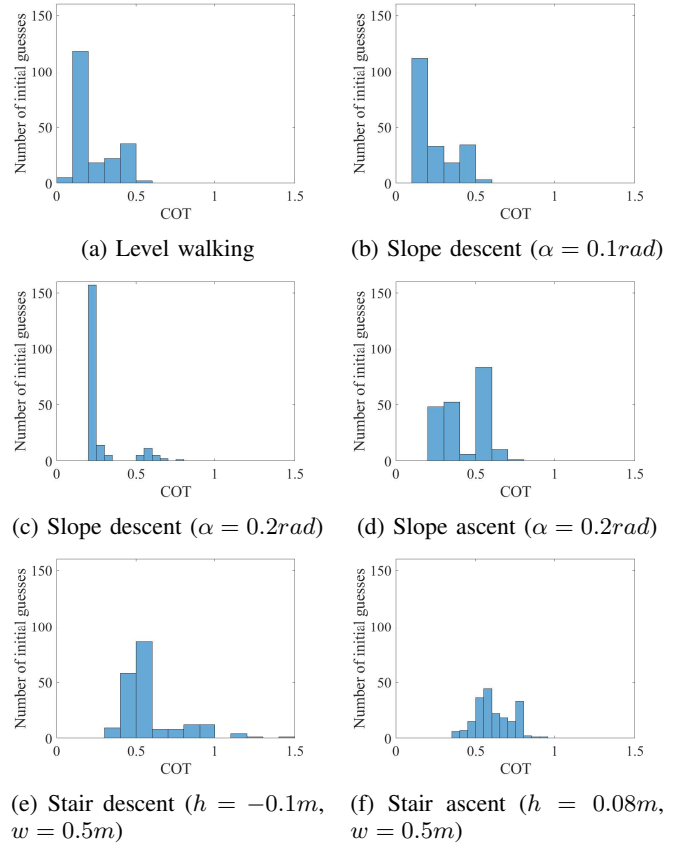


Fig. 6: The histograms of walking gaits on different terrains

of the optimization results, and present the distribution of COTs versus a set of initial guesses (where for each terrain, 200 randomized initial guesses generated using `rand()` in MATLAB were used to solve 200 gaits). The histogram can be a good indicator to show the optimization performance as well as the optimization complexity for each terrain. In Fig. 6 (a) for level walking, more than 100 initial guesses result in COTs lower than 0.2, which shows that the hybrid trajectory optimization can work with randomized initial guesses quite well. In addition, we found that when the downslope is steeper, the number of gaits having lower COTs increases. This seems reasonable because on a steeper slope, the larger potential energy can convert to the kinetic energy, and a local optimal solution with lower COT can then be more easily found. Conversely, when a walking gait needs to work against the gravity, the distribution becomes flatter (e.g., Fig. 6 (d)). This indicates it is possible but more difficult to get a great local optimal solution, and a better initial guess is more important in this case. Similarly, flat histograms can also be observed for stair walking as shown in Fig. 6 (e) and (f), where the nonsmooth  $\phi_z(q)$  make the optimization more difficult to be solved with low COT.

### D. Experiment Results

The level walking and downslope ( $5^\circ$ ) walking generated from the modified framework were tested on AMBER 3, where the gaits were achieved with consecutive steps. As shown in Figs. 7 and 8 and the video [1], the contact

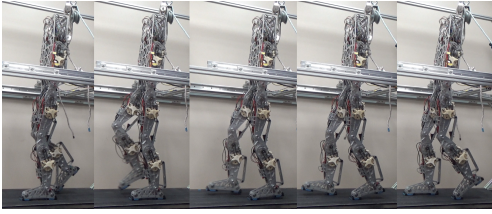


Fig. 7: The walking tiles of the level-walking experiment.

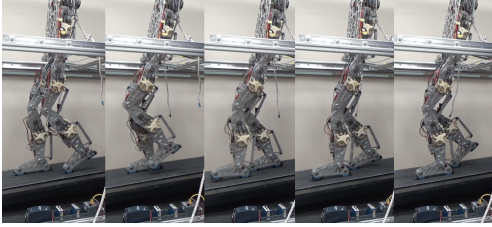


Fig. 8: The walking tiles of the downslope walking.

sequence of AMBER 3 matches the predefined contact sequence in Fig. 2. The phase portraits of the joint trajectories for the level walking and downslope walking are shown in Fig. 9, where the desired trajectories are from the optimization results. Although with the presence of disturbances such as joint frictions, the fluctuation of the treadmill speed, and the lateral support may push or drag the robot, those phase portraits can show that the experiment results are similar to the optimization results, which validate the framework with the generalized contact constraints.

## VI. CONCLUSIONS AND FUTURE WORK

In this work, we presented the generalized contact constraints for hybrid trajectory optimization to generate walking gaits on various terrains. With the modified contact constraints, this optimization framework can generate walking gaits on flat terrain, slopes, or stairs with different profiles, where the resulting gaits are compared and discussed. We also presented the histograms of optimization results with randomized initial guesses, which indicate the performance and the complexities of the optimization for different terrain profiles. The experimental results are also presented as validations. In the future, we plan to use this optimization framework to build a gait library to create more complex behaviors, and use it with the model of the human and lower-limb prosthesis to generate walking gaits for amputees.

## REFERENCES

- [1] Walking with foot rolling motion on AMBER 3: Visualizations and Experiments. <https://youtu.be/Y40nhmHMIBs>.
- [2] J. T. Betts. *Practical Methods for Optimal Control and Estimation Using Nonlinear Programming*. Society for Industrial and Applied Mathematics (SIAM), 2010.
- [3] P. A. Bhounsule, J. Cortell, A. Grewal, B. Hendriksen, J. G. D. Karssen, C. Paul, and A. Ruina. Low-bandwidth reflex-based control for lower power walking: 65 km on a single battery charge. *The International Journal of Robotics Research (IJRR)*, 33(10):1305–1321, 2014.
- [4] K. Chao and P. Hur. A step towards generating human-like walking gait via trajectory optimization through contact for a bipedal robot with one-sided springs on toes. In *IEEE/RSJ International Conference on Intelligent Robots and Systems (IROS)*, pages 4848–4853, Sept. 2017.

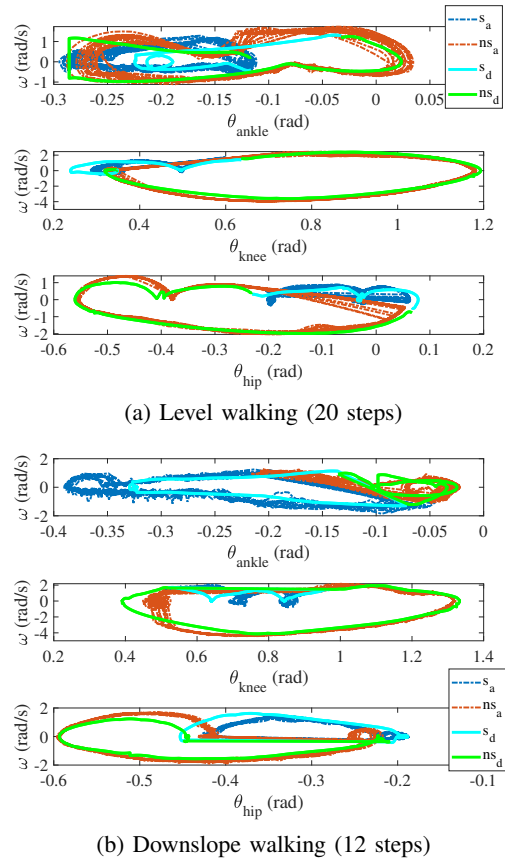


Fig. 9: The phase portraits of the walking gaits. In the legend, 's' and 'ns' indicate 'stance' and 'non-stance' respectively, and the subscript 'a' and 'd' indicate 'actual' and 'desired' respectively.

- [5] A. Hereid, E. A. Cousineau, C. M. Hubicki, and A. D. Ames. 3D dynamic walking with underactuated humanoid robots: A direct collocation framework for optimizing hybrid zero dynamics. In *IEEE International Conference on Robotics and Automation (ICRA)*, pages 1447–1454, May 2016.
- [6] A. Hereid, C. M. Hubicki, E. A. Cousineau, and A. D. Ames. Dynamic humanoid locomotion: A scalable formulation for HZD gait optimization. *IEEE Transactions on Robotics*, 34(2):370–387, 2018.
- [7] M. Kelly. An introduction to trajectory optimization: How to do your own direct collocation. *SIAM Review*, 59(4):849–904, 2017.
- [8] Z. Manchester and S. Kuindersma. Variational contact-implicit trajectory optimization. In *International Symposium on Robotics Research (ISRR)*, pages 4848–4853, Dec. 2017.
- [9] A. E. Martin, D. C. Post, and J. P. Schmiedeler. Design and experimental implementation of a hybrid zero dynamics-based controller for planar bipeds with curved feet. *The International Journal of Robotics Research (IJRR)*, 33(7):988–1005, 2014.
- [10] M. Posa, C. Cantu, and R. Tedrake. A direct method for trajectory optimization of rigid bodies through contact. *The International Journal of Robotics Research (IJRR)*, 33(1):69–81, 2014.
- [11] R. Riener, M. Rabuffetti, and C. Frigo. Stair ascent and descent at different inclinations. *Gait & Posture*, 15(1):32 – 44, 2002.
- [12] E. Westervelt and J. Grizzle. *Feedback Control of Dynamic Bipedal Robot Locomotion*. CRC Press, 2007.
- [13] E. R. Westervelt, J. W. Grizzle, and D. E. Koditschek. Hybrid zero dynamics of planar biped walkers. *IEEE Transactions on Automatic Control*, 48(1):42–56, 2003.
- [14] H. Zhao, A. Hereid, E. Ambrose, and A. D. Ames. 3D multi-contact gait design for prostheses: Hybrid system models, virtual constraints and two-step direct collocation. In *IEEE Conference on Decision and Control (CDC)*, pages 3668–3674, Dec. 2016.